Long-Term Sea Surface Temperature Variability along the U.S. East Coast

R. KIPP SHEARMAN

College of Oceanic and Atmospheric Sciences, Oregon State University, Corvallis, Oregon

STEVEN J. LENTZ

Woods Hole Oceanographic Institution, Woods Hole, Massachusetts

(Manuscript received 16 June 2009, in final form 2 December 2009)

ABSTRACT

Sea surface temperature variations along the entire U.S. East Coast from 1875 to 2007 are characterized using a collection of historical observations from lighthouses and lightships combined with recent buoy and shore-based measurements. Long-term coastal temperature trends are warming in the Gulf of Maine [1.0° ± 0.3°C (100 yr)$^{-1}$] and Middle Atlantic Bight [0.7° ± 0.3°C (100 yr)$^{-1}$], whereas trends are weakly cooling or not significant in the South Atlantic Bight [−0.1° ± 0.3°C (100 yr)$^{-1}$] and off Florida [−0.3° ± 0.2°C (100 yr)$^{-1}$]. Over the last century, temperatures along the northeastern U.S. coast have warmed at a rate 1.8–2.5 times the regional atmospheric temperature trend but are comparable to warming rates for the Arctic and Labrador, the source of coastal ocean waters north of Cape Hatteras (36°N). South of Cape Hatteras, coastal ocean temperature trends match the regional atmospheric temperature trend. The observations and a simple model show that along-shelf transport, associated with the mean coastal current system running from Labrador to Cape Hatteras, is the mechanism controlling long-term temperature changes for this region and not the local air–sea exchange of heat.

1. Introduction

Observational studies of climate variability in the ocean have necessarily focused on large-basin-scale behavior (e.g., Levitus et al. 2000) to ensure sufficient data coverage. Several high-quality, coarsely gridded (typically 2° × 2°) historical temperature analyses are available (e.g., Smith et al. 2008). The coastal ocean, however, is not well represented by these data products, because it is too narrow (less than 100 km wide), heavily populated with small-scale features (such as bays and estuaries; submarine banks and canyons; and fronts caused by tidal mixing, upwelling, and other processes), and governed by dynamics and circulation that are distinctly different from the larger-scale basin circulation resolved by the gridded data products. Thus, observational records from the coastal ocean that span a century or even several decades (e.g., Mountain 2003) are extremely valuable. Understanding the physical processes that contribute to the interannual and long-term climate-scale variability of temperature in the coastal ocean is important, because temperature plays a key role in coastal ecosystems, affecting the timing of the spring phytoplankton bloom and the livable habitat range and spawning behaviors of important commercial species (Valiela 1995).

Beginning in 1820, the U.S. government established permanently moored ships, equipped with light beacons, along the U.S. coastline to serve as floating lighthouses in areas where fog, currents, or shoals might pose a danger to passing ships (Flint 1989, 1993). Around 1873, lightship (and some lighthouse) keepers began regularly collecting meteorological and oceanographic observations (Bumpus 1957). Lightships were gradually retired because advances in technology made navigation more reliable and the observational duties were taken up by autonomous moored buoys and shore stations operated by the National Oceanic and Atmospheric Administration (NOAA). In addition to lightship and buoy observations, several long-running sea surface temperature (SST) observations have been made at tide stations (U.S. Coast and Geodetic Survey 1955) and independent institutions, such as the Woods Hole Oceanographic Institution (Nixon et al. 2004). The merger of these historical and recent

Corresponding author address: R. Kipp Shearman, College of Oceanic and Atmospheric Sciences, Oregon State University, 104 COAS Admin. Bldg., Corvallis, OR 97331.
E-mail: shearman@coas.oregonstate.edu

DOI: 10.1175/2009JPO4300.1

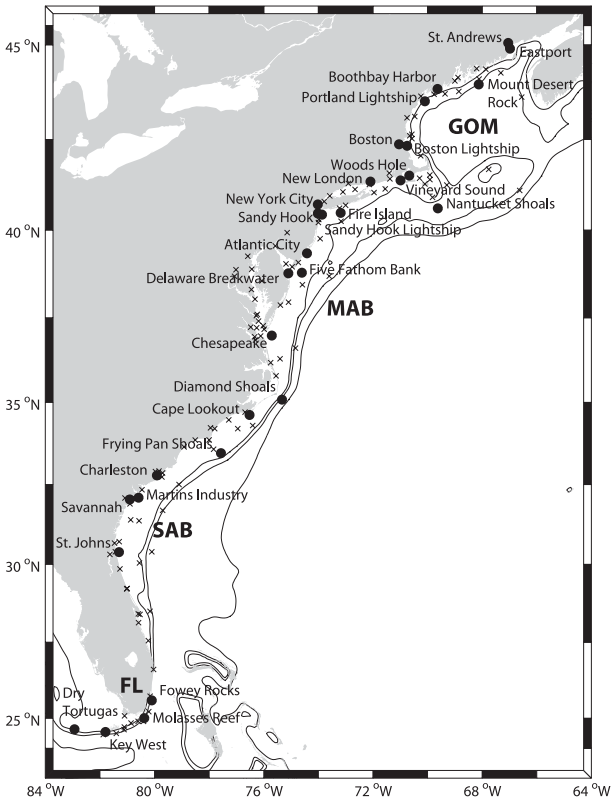

FIG. 1. Map of the U.S. East Coast showing the sites of the merged historical and recent temperature observations (crosses) and the 30 longest data-rich sites (circles and labels). In addition, coastal regions are labeled: GOM, MAB, SAB, and southern FL. The 40-, 100-, and 1000-m isobaths are contoured.

observations presents a unique opportunity to evaluate the long-term temperature variability over the continental shelf along the entire U.S. East Coast.

2. Background

a. Circulation along the U.S. East Coast

The coastal ocean along the U.S. eastern seaboard can be separated into three distinct regions (Fig. 1): the Gulf of Maine (GOM), Middle Atlantic Bight (MAB) and South Atlantic Bight (SAB). The mean circulation within the MAB and GOM is part of a large-scale coastal current system that originates in the Arctic Ocean (Chapman and Beardsley 1989), flowing at approximately 10–20 cm s^{-1} southward along the shelf past Labrador, Canada, and around the Grand Banks (Fratantoni and Pickart 2007; Lentz 2008; Loder et al. 1998). In contrast, the mean circulation within the SAB is weaker and less directionally resolute. The currents near the shelf break are strongly influenced by the northward-flowing Gulf Stream (Lee et al. 1984), but there are indications of southward flow near the coast driven by local river runoff (Boicourt et al. 1998). There is almost no exchange of water between the MAB and SAB, with the dividing point at Cape Hatteras, North Carolina (Pietrafesa et al. 1994).

b. Long-term temperature variability in the coastal ocean

On long time scales, the coastal ocean is generally thought to be in thermal equilibrium with the atmosphere, controlled by latent, sensible, and net longwave radiative surface heat fluxes, which are all strong functions of the atmosphere–ocean temperature difference (Fairall et al. 1996; Fung et al. 1984). In this case, one might expect coastal ocean temperatures to track the long-term regional atmospheric temperature fluctuations. Unfortunately, little is known about long-term temperature variability in the coastal ocean or how it relates to atmospheric temperatures, and the few existing data records are confusing and inconsistent. Previous studies have identified long-term coastal SST trends ranging from $-0.1°$ to 4.0°C $(100\ yr)^{-1}$ but with no discernable pattern or relation to the atmospheric temperatures (Maul et al. 2001; Nixon et al. 2004). However, an early examination of lightship temperature records from 1873 to 1961 found a general trend toward warmer SSTs that peaked around 1950 and diminished toward the south (Stearns 1965) but without direct comparison with atmospheric temperatures. Recent studies have found along-shelf advection to be a significant contribution to the mean heat budget along the MAB shelf (Lentz 2010).

3. The dataset

The data for this analysis are composed of historical observations from lightship, lighthouse, and tide station records (Bumpus 1957; U.S. Coast and Geodetic Survey 1955); they are compiled and digitized from the original records at the Woods Hole Oceanographic Institution (available online at http://www.whoi.edu/science/GG/woos/index.html), and more recent observations from NOAA buoys and shore sites are accessed through the National Data Buoy Center (NDBC). These data include sea surface temperature records from individual institutions, such as the Woods Hole Oceanographic Institution and the Department of Fisheries and Oceans Canada, and from the growing facilities of regional coastal ocean observing systems. The sites span the length of the entire U.S. eastern seaboard and include measurements from bays and estuaries, the open coastline, and across the continental shelf (Fig. 1). It is important to note that the historical observations presented here have not been integrated into the international community databases, such as the International Comprehensive Ocean–Atmosphere

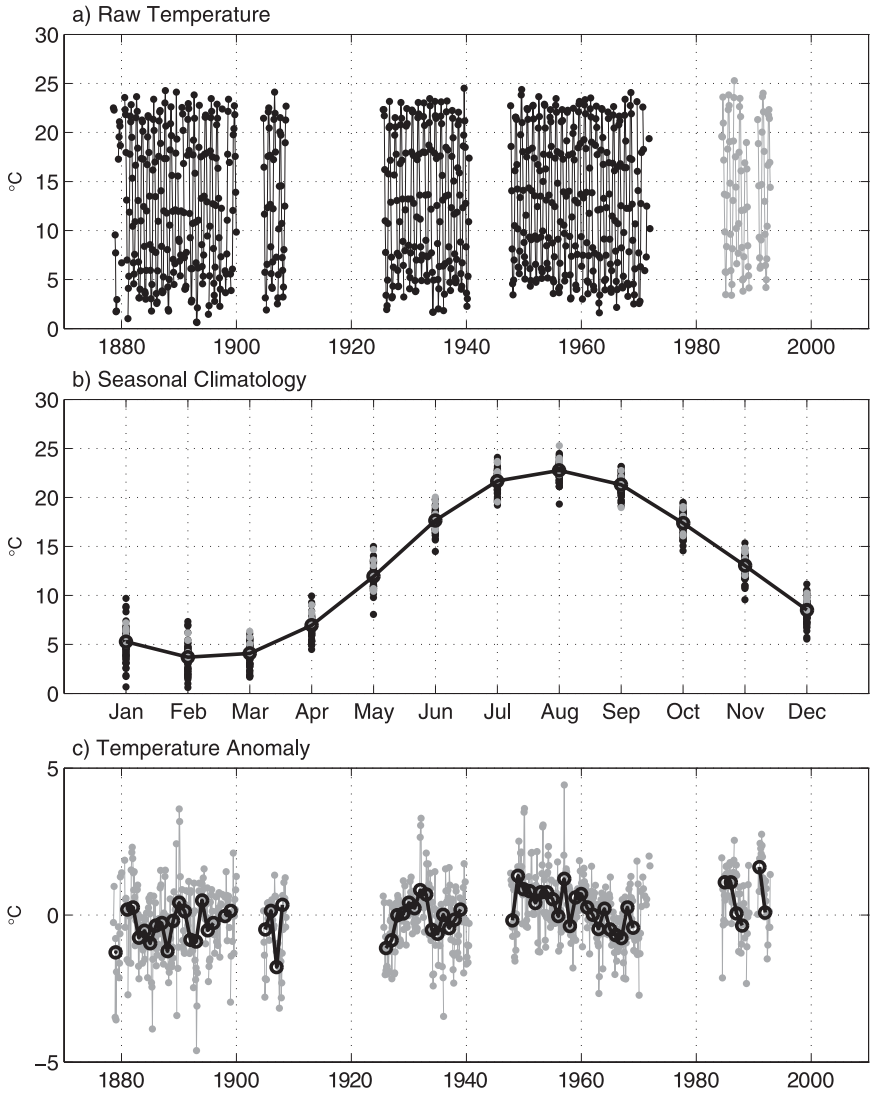

FIG. 2. (a) Raw monthly temperature time series from the Five Fathom Bank Lightship (black) and NDBC buoy 44015 (gray), which occupy the same position and are directly merged; (b) raw temperature observations by month and monthly climatology (thick black line); and (c) monthly anomalies (gray) and annual average anomalies (black).

Data Set (ICOADS; Worley et al. 2005); approximately 1% of the historical (pre-1970) observations presented here are duplicated in the ICOADS individual marine reports.

Historical observations were collected 1–6 times per day, at fixed times or times fixed to local tidal phase, using a bucket and thermometer up until 1970. The NDBC buoy observations were collected hourly, using paired electronic thermistors, beginning around 1975 (NDBC 2003). A few historical sites introduced electronic sampling before 1970, such as Boothbay Harbor (Bumpus 1957). If a lightship or buoy changed position, it was treated as a new site. The daily observations were averaged to form time series of monthly values at every site (when at least 23 days were available). A small number of monthly averages were discarded because they fell below −2.0°C, the freezing point of saline coastal waters. Along-shelf coordinate system and positions for all sites were estimated from the closest point along the 40-m isobath (Fig. 1), increasing to the south.

a. Merging historical and recent data

Sometimes, historical observation sites were replaced with NDBC buoys or shore stations; in this case, the time series are directly merged (e.g., Fig. 2a). Approximately 12% of the sites are the result of direct merger. If sites are

geographically close (<30 km), come from a similar water depth (±10 m) and coastal setting (classified as bays, open coast, and shelf), and have similar seasonal cycles (±1°C), then those sites are merged to form a single time series at the location of the site with the most observations. An adjustment of −1.0°C per degree latitude (estimated by linear fit to the mean SSTs) is added to observations from the site that is moved to compensate for the northward decrease in mean temperature. Approximately 27% of the sites are the result of geographically similar merger. Any remaining sites with less than 3 yr of data are excluded from this analysis.

The seasonal cycle for each site is estimated as monthly climatological averages (e.g., Fig. 2b). Monthly anomalies from the climatological average at each site are calculated, and annual average anomalies are computed when at least 9 months are available in a year (e.g., Fig. 2c). Winter [January–March (JFM)], spring (April–June), summer [July–September (JAS)], and fall (October–December) seasonal anomalies are computed, when at least 2 months are available in a season.

The final dataset includes 128 sites along the U.S. East Coast from Eastport, Maine, to Dry Tortugas, Florida (FL; Fig. 1), spanning the years from 1875 to 2007. Of these, 46 sites have more than 25 yr of observations, 15 sites have more than 50 yr of observations, and 4 sites have more than 75 yr of observations. A total of 30 time series are chosen for length and completeness over the last century to estimate long-term trends (Fig. 1, labeled sites).

The remarkable achievement represented by the early lightship and lightstation observations is apparent when we compare the number of observation sites along the East Coast through time. Only recently (since 2005) have the total number of sites (all autonomous buoys and shore stations) producing a full year of observations exceeded the peak from 1880 to 1890 (Fig. 3), when observations were made by hand using buckets and thermometers. The human effort required to maintain such a network of observations is impressive.

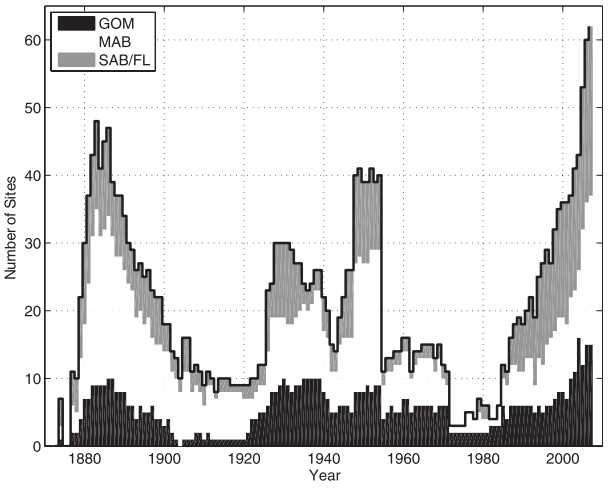

FIG. 3. Number of sites along the U.S. East Coast returning a full year of observations from 1875 to 2007. The different coastal regions are shaded. The peak achieved from 1880 to 1890, when observations were made by hand using a bucket and thermometer, was not equaled until 2005, when observations were completely automated.

b. Accuracy

The accuracy of SST measurements made on NDBC buoys using electronic thermistors is ±0.08°C for an individual hourly measurement, based on duplicate sensor comparisons (NDBC 2003), and therefore the standard error for a monthly average is quite small. The accuracy of bucket temperature measurements is more complicated. The error associated with thermometers readings has been shown to be negligible for a monthly average (Maul et al. 2001). However, bucket temperature measurements suffer from a well-known bias toward cooler temperatures compared to modern thermistors observations (Folland 2005; Folland and Parker 1995; Smith and Reynolds 2002). The full details of our bucket temperature bias correction and the improvement obtained in the corrected data are contained in the appendix. Other factors, such as sample depth, number of observations per day, and timing of observations, can decrease the accuracy of SST measurements, but these effects are generally negligible for annual and seasonal averages (Folland and Parker 1995; Maul et al. 2001; Nixon et al. 2004).

c. Atmospheric surface temperature

To address the role of the atmosphere in driving coastal ocean temperatures, we need to characterize the larger, regional-scale atmospheric temperature variability. Atmospheric surface temperature data for comparison with coastal historical temperature observations come from two sources. The first source is the U.S. Historical Climatology Network for the northeast (Connecticut, Delaware, Maine, Maryland, Massachusetts, New Hampshire, New York, Pennsylvania, Rhode Island, and Vermont) and southeast (Alabama, Florida, Georgia, North Carolina, South Carolina, and Virginia) U.S. regions (Easterling et al. 1996; Williams et al. 2007), which consists of monthly average temperatures for the regions. We compute monthly, seasonal, and annual anomalies from these data following the steps outlined for coastal SSTs (obviously, no bucket correction is applied). The second source is the merged land, air, and sea surface temperature anomaly analysis from the Global Historical Climatology Network and ICOADS (Smith and Reynolds 2005; Smith et al. 2008). The data consist of monthly

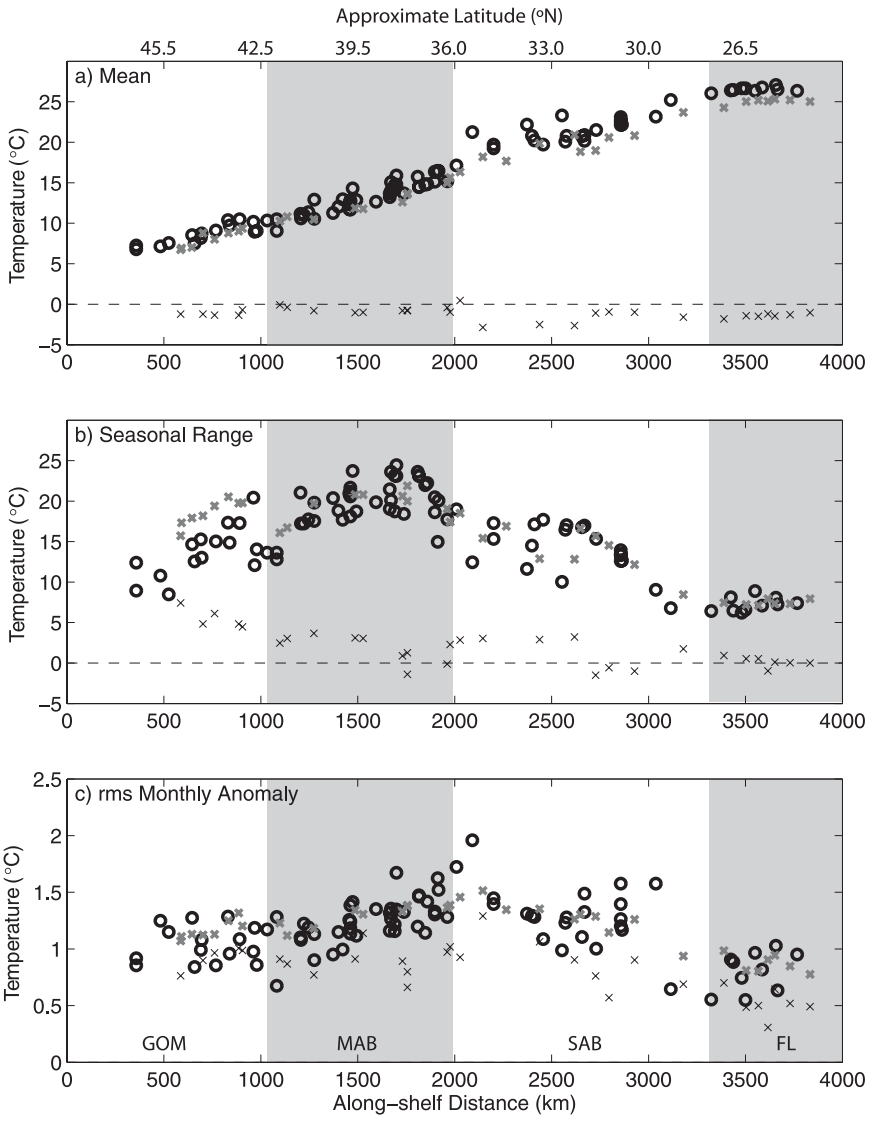

FIG. 4. (a) Mean temperature, (b) seasonal cycle range, (August–February difference), and (c) rms variability of the monthly temperature anomaly for coastal ocean SST (black circles), NDBC buoy atmospheric temperature (gray crosses), and atmosphere–ocean temperature difference (black crosses). Along-shelf regions are shaded.

anomalies on a 5° latitude × 5° longitude grid, and we compute seasonal and annual anomalies. We use five grid points over Labrador to represent the long-term surface temperature variability there.

In addition to the regional-scale atmospheric temperature variability, NDBC buoy observations in the coastal ocean often (70%) have atmospheric temperature observations on hourly intervals (among other atmospheric observations). The NDBC buoy atmospheric temperature observations span from about 1975 to the present. From the hourly observations, we compute monthly averages of coastal atmospheric temperature and atmosphere–ocean temperature difference; from the monthly averages, we compute monthly, seasonal, and annual anomalies following the same process as for coastal SSTs (again, no bucket correction for atmospheric temperatures or modern SSTs).

4. Results

Mean coastal SSTs increase to the south (in the positive along-shelf direction) at a rate of 6.4×10^{-3} °C km^{-1} (−1.0°C per degree latitude) from about 7°C in the GOM to 27°C off FL (Fig. 4a). Mean coastal atmospheric temperatures also increase to the south at a slightly lower rate of 6.0×10^{-3} °C km^{-1}, and coastal atmospheric

temperatures are on average about 1.3°C cooler than coastal SSTs. The seasonal cycle range, estimated as the difference between the August and February climatological averages, increases from about 10°C in the GOM to a maximum of 23°C in the MAB and then decreases to a minimum of 7°C off FL (Fig. 4b). The seasonal range of coastal atmospheric temperature follows a similar pattern. The seasonal range of the atmosphere–ocean temperature difference is largest in the GOM (5.5°C), decreases to the south, and is weakest off FL (0.2°C). The rms variability of monthly coastal SST anomalies ranges from 0.6° to 2.0°C but has no along-shelf or latitudinal dependence (Fig. 4c). The maximum occurs at the Diamond Shoals Lightship (35°N), which may reflect the influence of the nearby Gulf Stream. On average, rms variability decreases slightly from sites classified as bays (1.29° ± 0.05°C) to open coasts (1.17° ± 0.04°C) to the continental shelf (0.98° ± 0.04°C). The rms variability of monthly coastal atmospheric temperature anomalies is nearly identical in magnitude and structure to the coastal SST anomalies: likewise for the rms variability of the atmosphere–ocean monthly anomalies, only with a general decrease in magnitude.

a. Long-term SST variability

Average SSTs along the U.S. East Coast north of Cape Hatteras (36°N) have warmed over the last 100-plus yr, whereas SSTs to the south have effectively remained constant or cooled slightly. North of Cape Hatteras, the average temperatures from 1980 to 2005 are 0.5°–1.3°C warmer than the average temperatures a century earlier from 1880 to 1905 (Table 1). South of Cape Hatteras, average temperatures from 1980 to 2005 compared to those from 1880 to 1905 (Table 1) have increased at one site (Savannah), registered no change at two sites (Cape Lookout and Fowey Rocks), and decreased at four sites (Martins Industry Lightship, Molasses Reef, Key West, and Dry Tortugas).

Likewise, annual average SST anomalies from Eastport to the Chesapeake Lightship (in the MAB and GOM) reflect this long-term temperature increase with a tendency for positive temperature anomalies after 1940 compared to sites in the SAB and FL from the Diamond Shoals Lightship to Dry Tortugas (Fig. 5). If we identify the five warmest years at each site, 92% occur after 1940, with ⅓ of those occurring during the warm 1950s and another ⅓ occurring after 2000. In addition, annual average anomalies are correlated at interannual to decadal time scales over large along-shelf distances, cross-shelf position, and across different coastal settings (bays, open coast, and shelf). For example, an extended warm period during the 1950s and the exceptionally warm 2002 are identifiable at nearly every site (Fig. 5).

TABLE 1. Average SSTs from 1880 to 1905 compared to average SSTs from 1980 to 2005.

Station	Mean 1880–1905	No. of years	Mean 1980–2005	No. of years	ΔT (°C)
Eastport	6.5	10	7.2	9	0.7
St. Andrews	—	—	7.3	23	—
Mt. Desert Rock	7.3	12	7.9	4	0.6
Boothbay Harbor	7.9*	20*	9.0	23	1.1
Portland Lightship	8.1	8	9.0	21	0.9
Boston	9.9	8	10.7	7	0.8
Boston Lightship	—	—	9.9	19	—
Nantucket Shoals	9.8	4	11.0	21	1.2
Woods Hole	10.8	23	11.7	25	0.9
Vineyard Sound	10.2	23	11.4	7	1.2
New London	12.6	7	—	—	—
Fire Island	12.1	6	12.7	15	0.6
New York City	11.9	8	13.2	8	1.3
Sandy Hook Lightship	12.0	12	12.5	12	0.5
Sandy Hook	12.3	11	13.0	5	0.7
Atlantic City	12.8	16	—	—	—
Five Fathom Bank	13.0	19	13.5	6	0.5
Delaware Breakwater	13.8	23	—	—	—
Chesapeake	—	—	15.4	17	—
Diamond Shoals	—	—	21.2	9	—
Cape Lookout	19.2	18	19.2	11	0.0
Frying Pan Shoals	—	—	22.2	8	—
Charleston	20.8	9	—	—	—
Martins Industry	20.8	21	20.3	7	−0.5
Savannah	20.2	6	21.4	4	1.2
St. Johns	—	—	21.9	5	—
Fowey Rocks	26.5	21	26.5	14	0.0
Molasses Reef	26.9	17	26.6	20	−0.3
Key West	26.7	9	26.3	8	−0.4
Dry Tortugas	26.4	24	26.1	9	−0.3

* Average over period from 1900 to 1925.

Annual average anomalies (detrended) are correlated over large along-shelf distances (Fig. 6). The along-shelf decorrelation length scale is about 2500 km, approximated as the zero crossing of the line fit to the correlation estimates. However, there is a significant drop in correlation between sites on opposite sides of Cape Hatteras. Correlations between two sites that are either both north and both south of Cape Hatteras are larger than correlations between two sites that span Cape Hatteras. At short separations (less than 1500 km), bin-averaged correlations are significantly smaller for sites that span Cape Hatteras than for sites that do not (Fig. 6), ignoring correlations of 1.0 at 0-km separation. The large correlation length scales suggest a large-scale forcing mechanism, but the drop in correlation across Cape Hatteras suggests that the dominant forcing mechanism may be different for these two regions.

b. Long-term SST trends

The north–south dichotomy is also reflected in the long-term SST trends. North of Cape Hatteras, long-term

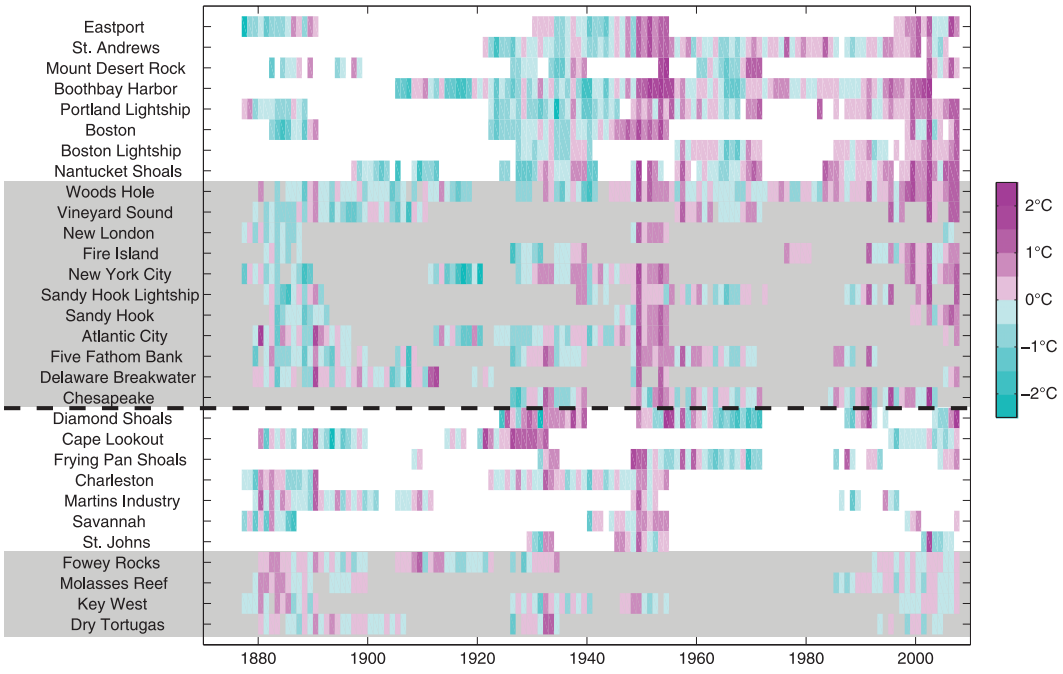

FIG. 5. Annual average SST anomalies (section 3a) along the U.S. East Coast. Along-shelf regions are shaded, and the dashed line indicates the approximate position of Cape Hatteras (36°N).

trends estimated from the annual average anomalies are all warming; south of Cape Hatteras, long-term trends are mostly cooling (Fig. 7). In the GOM and MAB, 15 of 19 sites exhibit a warming trend that is significantly different from zero, ranging from 0.6° to 1.5°C (100 yr)$^{-1}$. Confidence intervals for linear trends are at the 95% level and are estimated using a Student's t test, with each annual anomaly treated as an independent point (results do not qualitatively change for 3- or 5-yr averages). In the SAB and FL, only 2 of 11 sites are significantly different from zero: one indicates warming and the other indicates cooling. Furthermore, in the GOM and MAB, most of the warming occurs during the wintertime. Long-term trends for the winter season (JFM) SST anomalies are on average 0.5° ± 0.2°C (100 yr)$^{-1}$ larger than summer season (JAS) trends. For the SAB and FL, there is no significant difference between wintertime and summertime trends [−0.1° ± 0.1°C (100 yr)$^{-1}$].

c. *Comparison with atmospheric surface temperatures*

Given the large spatial scales associated with the annual average SST anomalies, we compute composite averages for the GOM (Eastport to Nantucket Shoals), MAB (Woods Hole to Chesapeake Lightship), SAB (Diamond Shoals Lightship to St. Johns Lightship), and FL (Fowey Rocks to Dry Tortugas) to compare with the large-scale regional atmospheric temperatures. Composite averages are computed from all available time series in that region with a common time period mean removed; if only one time series is available for a given year, that single value is used. The GOM and MAB composite average SST anomalies are warming at 1.0° ± 0.3° (95% confidence interval) and 0.7° ± 0.3°C (100 yr)$^{-1}$, respectively (Fig. 8). The long-term trend in the SAB is not significantly different from zero, −0.1° ± 0.3°C (100 yr)$^{-1}$, whereas the FL trend indicates barely significant, weak cooling of −0.3° ± 0.2°C (100 yr)$^{-1}$.

The long-term SST trends in the GOM and MAB are 1.8–2.5 times greater than the northeast U.S. regional air temperature trend of 0.4° ± 0.4°C (100 yr)$^{-1}$ but are similar to the air temperature trend of 1.1° ± 0.4°C (100 yr)$^{-1}$ for Labrador. The larger trend is also comparable to surface temperature trends in the Arctic (Steele et al. 2008; Trenberth et al. 2007). The long-term SST trends in the SAB and FL are comparable to the lack of significant trend in the southeast U.S. regional air temperatures, −0.1° ± 0.3°C (100 yr)$^{-1}$.

5. Discussion

The fact that coastal SSTs regionally exhibit similar trends and are correlated over large along-shelf length scales is consistent with a large-scale forcing mechanism. There is an obvious change near Cape Hatteras, with warming to the north that exceeds the northeast U.S.

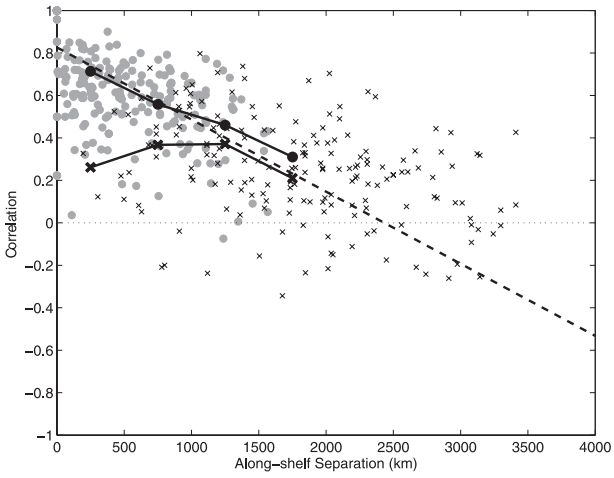

FIG. 6. Correlation of annual average SST anomalies (section 3a) as a function of along-shelf separation. Correlation estimates from two sites that span Cape Hatteras (36°N) are shown by thin crosses, whereas correlations from two sites that do not span Cape Hatteras are shown by gray circles. Bin-averaged (500-km bins) correlations are show by thick crosses (span Cape Hatteras) and black circles (do not span Cape Hatteras). The zero crossing (~2500 km) from a line fit to the correlation estimates (thick dashed line) is used to approximate the decorrelation length scale.

regional trend but matches the trend over Labrador and in the Arctic and little or no change to the south that matches the lack of trend in the southeast U.S. regional atmospheric temperature. Cape Hatteras also marks the point where the mean southward along-shelf flow through the GOM and MAB ends. It seems likely then that different processes dominate north and south of Cape Hatteras.

Surface air–sea heat fluxes can affect SSTs coherently over large atmospheric scales. Sensible, latent, and net longwave surface heat fluxes depend to some extent on the ocean–atmosphere temperature difference, so large-scale changes in atmospheric surface temperatures can impact coastal SSTs on similar scales (Mountain et al. 1996). If surface fluxes are the dominant mechanism, then average coastal ocean temperatures will track atmospheric temperatures after an initial adjustment period and long-term (100 yr) coastal ocean and atmospheric temperature trends will be identical. This assumes that the ocean achieves equilibrium with the atmosphere; the adjustment period is short compared to the long-term trend; and the atmosphere is an independent reservoir of heat, unaffected by temperature changes in the coastal ocean (a solid assumption given the infinitesimal volume of the coastal ocean compared to the volume of the regional-scale atmosphere). Along-shelf transport can also manifest long-term changes in the coastal ocean through changes in source water temperatures; if advection is the sole driver and source waters are warming, then everywhere downstream will be warming at the same rate. Here, we develop a simple model to examine the relative effects of surface heating and along-shelf advection on long-term coastal SST trends.

Along-shelf advection, surface heat flux, and long-term trends

Assuming a simple flat-bottom shelf geometry of depth H with constant along-shelf flow u, the cross-shelf and depth-averaged heat equation is

$$\frac{\partial T}{\partial t} + u\frac{\partial T}{\partial x} = \frac{Q}{\rho_o c_p H}, \tag{1}$$

where T is the average shelf temperature; (x, y, z) are the along-shelf, cross-shelf, and vertical coordinates; ρ_o is the average density (1024 kg m^{-3}); c_p is the specific heat of seawater (4190 J kg^{-1} K^{-1}); and Q is the total surface heat flux. This simple model ignores the cross-shelf heat flux at the offshore boundary resulting from advection or lateral mixing.

The total heat flux Q is the sum of the net shortwave and net longwave radiative heat fluxes and the sensible and latent heat fluxes. The net longwave, sensible, and latent heat fluxes are all strong linear functions of atmosphere–ocean temperature difference, and Q can be approximated by

$$Q = Q_{\mathrm{sw}} + \alpha(T_a - T) + Q_o, \tag{2}$$

where Q_{sw} is the constant net shortwave heat flux; T_a is the atmospheric temperature; and α and Q_o are determined by least squares fit to the sum of the net longwave, latent, and sensible heat fluxes, using the NDBC buoy data to make bulk heat flux estimates (Fairall et al. 1996). Equation (2) is an approximation, because the atmosphere–ocean temperature difference is estimated as the atmospheric temperature minus the average ocean temperature and not the sea surface temperature. The values of α range from 20 to 60 W m^{-2} K^{-1} and increase along-shelf to the south (Fig. 9). To capture the fundamental effects of long-term trends, the large-scale atmospheric temperature can be written

$$T_a = at + bx + T_{ao}, \tag{3}$$

where a is the long-term temperature trend; b is the constant along-shelf temperature gradient; and T_{ao} is the atmospheric temperature at $x = 0$, the source water location.

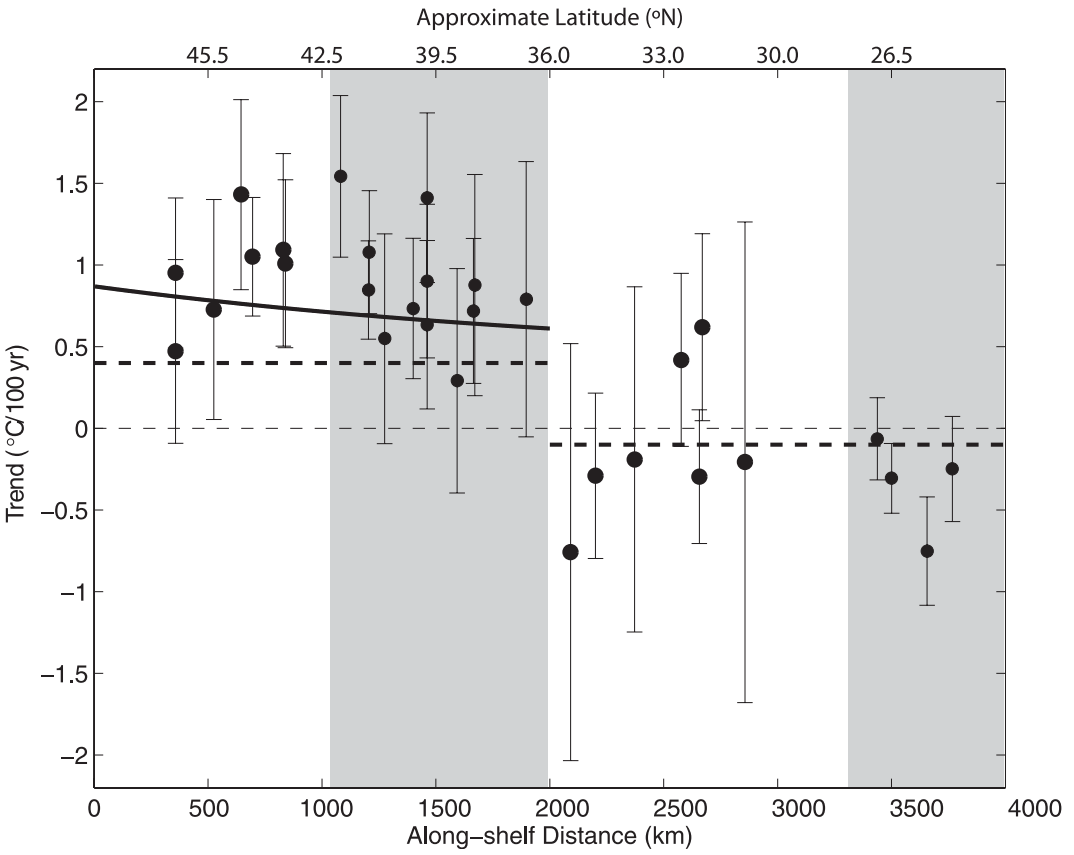

FIG. 7. Long-term coastal SST trends with 95% confidence intervals along the U.S. East Coast, computed by linear fit to the annual average anomalies, and results from the simple model without advection (thick dashed lines) and with advection (thick solid line). Coastal regions are shaded.

If advection is negligible and we use the initial condition $\partial T/\partial t = 0$ (ocean–atmosphere equilibrium), the solution for temperature is

$$T^{u=0}(x, t) = \tau a e^{-t/\tau} + T_a + (Q_{sw} + Q_o)\alpha^{-1} - \tau a, \quad (4)$$

where

$$\tau = \rho_o c_p H \alpha^{-1} \quad (5)$$

is the time scale for average coastal ocean temperatures to adjust to atmospheric temperature changes. Given the range of values on the northeast U.S. coast for α, given the constants ρ_o and c_p, and choosing an average shelf depth of 50–100 m, the adjustment time period is 60–240 days. This range of adjustment period is consistent with observed phase shifts over depth in temperature in the MAB (Lentz et al. 2003). For time periods that are much longer than the adjustment period, average coastal ocean temperature will track atmospheric temperature and the long-term trend will match identically; that is, for $t \gg \tau$,

$$\frac{\partial T^{u=0}}{\partial t} = a. \quad (6)$$

Using the simplified atmospheric forcing (2), the fundamental heat balance with advection (1), and a boundary condition specifying the long-term trend for source water temperature

$$T(0, t) = At + T_o, \quad (7)$$

an analytical solution for $T(x, t)$ can be found for $0 < x < ut$,

$$T(x, t) = [(A - a)(t - x/u) + T_o - T_{ao} + \tau(a + bu) - (Q_{sw} + Q_o)\alpha^{-1}]e^{-x/u\tau} + T_a + (Q_{sw} + Q_o)\alpha^{-1} - \tau(a + bu). \quad (8)$$

In this case, the evolution of average coastal ocean temperature is influenced by surface forcing (through

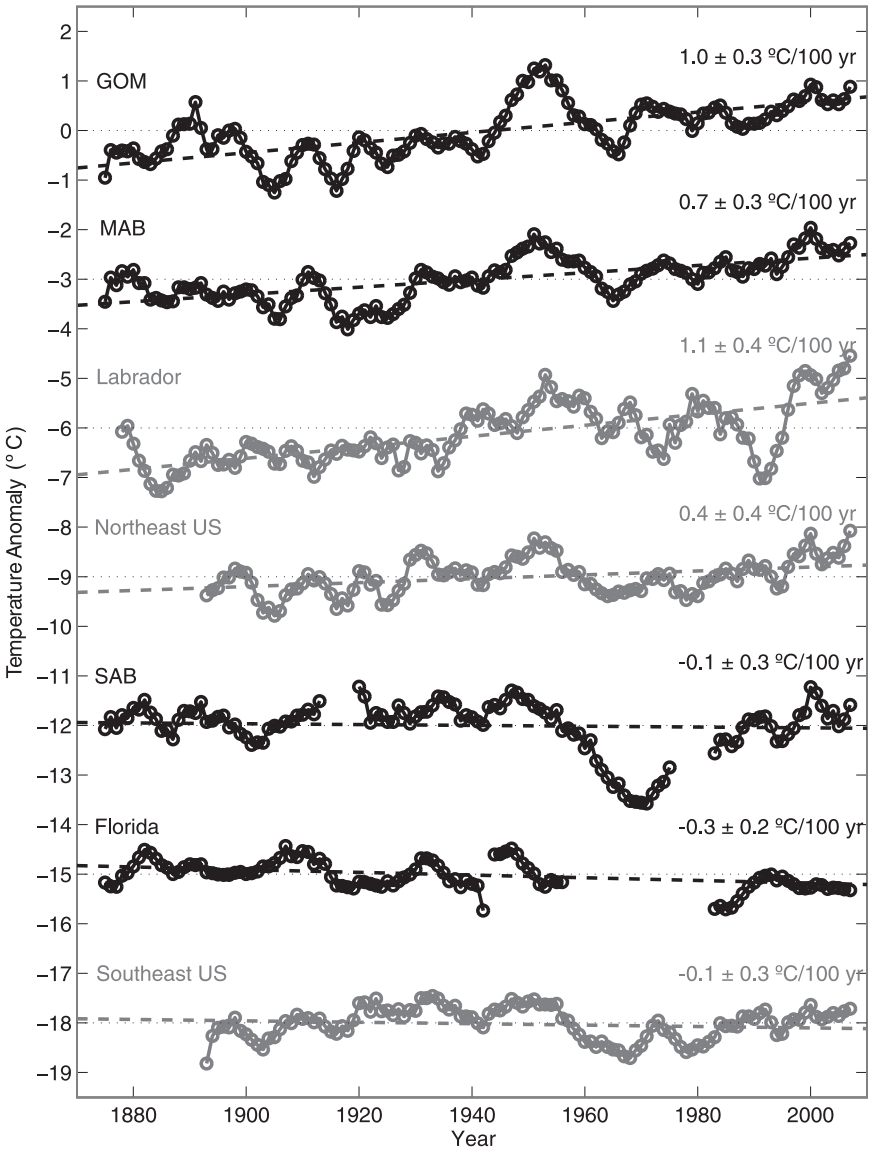

FIG. 8. Composite average SST anomalies (black) for GOM, MAB, SAB, and FL, smoothed with a 5-yr running mean, plus regional surface air temperature anomalies (gray) for the northeast United States, southeast United States, and Labrador. Best linear fits are plotted (thick dashed lines), and trends with 95% confidence intervals are noted.

atmospheric temperature changes) and the in-flow characteristics are determined by changes in source water temperature. The long-term coastal ocean temperature trend,

$$\frac{\partial T}{\partial t} = (A - a)e^{-x/u\tau} + a, \tag{9}$$

transitions from the source water trend A to the atmospheric trend a over the decay-scale distance $D = u\tau$. Along-shelf currents for the GOM and MAB are about 0.10 m s^{-1} (Lentz 2008), and shelf currents are typically stronger to the north, approaching 0.20 m s^{-1}, resulting in transition distances ranging from 600 to 4800 km. The distance from the northeast U.S. coast to the Labrador shelf is about 2000 km. This may also explain why long-term trends decrease moving from the GOM to the MAB, a distance of 1200 km.

Using the long-term atmospheric temperature trend over Labrador as the source water trend A and the northeast U.S. regional (0–2000 km) and the southeast U.S. regional (2000–4000 km) atmospheric temperature

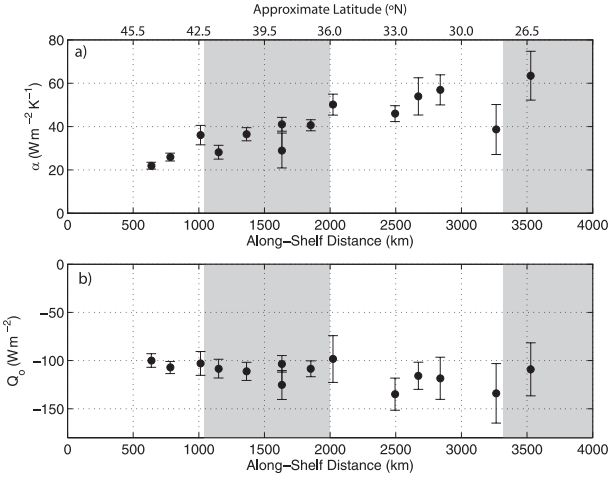

FIG. 9. Parameters (top) α and (bottom) Q_o used to approximate surface heat flux as a function of ocean–atmosphere temperature difference (2), estimated from NDBC buoy observations along the U.S. East Coast.

trends as the local surface forcing trend a, we compare the analytical solutions (parameters specified in Table 2) for average coastal ocean temperature trends with and without advection to the observed long-term trends (Fig. 7). Without advection, the analytical solution (4) reverts to the local surface forcing trend a; north of Cape Hatteras, this value is clearly low, whereas it is more similar south of Cape Hatteras. The analytical solution with advection (9) results in long-term coastal ocean temperature trends between the source water trend A and local surface forcing trend a, with an average warming rate for region north of Cape Hatteras of 0.7°C $(100\ \text{yr})^{-1}$. The comparison is, of course, not exact; however, the ability of the highly simplified model to reproduce the observed enhanced warming north of Cape Hatteras is striking.

The similarity with long-term trends over Labrador, the mean southward along-shelf flow, and the approximate adjustment distances in the simple advective model suggest that along-shelf transport, not surface heat flux, is controlling the long-term temperature variability in the GOM and MAB. Source waters off Labrador are presumably warming in balance with the long-term atmospheric trends there and advecting south through the GOM and MAB, leaving at Cape Hatteras and having no effect farther south, where both coastal SSTs and atmospheric temperatures lack significant long-term trends. No other mechanism is likely to achieve this dichotomy of behavior.

6. Conclusions

Historical SST observations from lightships and lighthouses, combined with recent buoy and shore station observations, show significant long-term warming along the northeast U.S. coast and no significant trend along the southeast coast. To the north of Cape Hatteras, SSTs are warming at a rate 1.8–2.5 times larger than the regional atmospheric temperature trend but similar to atmospheric trends over Labrador and the Arctic, the source waters for the GOM and MAB. This suggests that along-shelf transport results in coastal ocean warming that exceeds local atmospheric temperature increases. Thus, changes in ice cover (Stroeve et al. 2007) and continued Arctic warming (Steele et al. 2008; Trenberth et al. 2007) could have a profound impact on the northeast U.S. coastal ocean, because temperature plays a key role in coastal ecosystems, affecting livable habitat ranges and spawning behaviors of commercially important species.

Acknowledgments. We thank Kathryn Elder (WHOI) for digitizing historical lightship temperature records. This work was supported by NSF Grant OCE-0220773.

TABLE 2. Parameter values used to solve for long-term temperature trends [Eqs. (6) and (9)].

Parameter	Definition	Value
x_o	In-flow boundary location in true coordinate system	−2000 km
A	Source water trend	1.1°C $(100\ \text{yr})^{-1}$
a	Regional atmospheric trends	0.4°C $(100\ \text{yr})^{-1}$; $x < 2000$ km; -0.1°C $(100\ \text{yr})^{-1}$; $2000 < x < 4000$ km;
u	Along-shelf current	0.15 m s^{-1}; $x < 2000$ km; 0.0 m s^{-1}; $2000 < x < 4000$ km
ρ_o	Mean density	1024 kg m^{-3}
c_p	Specific heat of coastal water	4190 J kg^{-1} K^{-1}
H	Shelf depth	80 m
α	Surface heat flux parameterization (2)	20 W m^{-2} K^{-1}
τ	$\tau = \rho_o c_p H \alpha^{-1}$	198 days
D	$D = u\tau$	2570 km

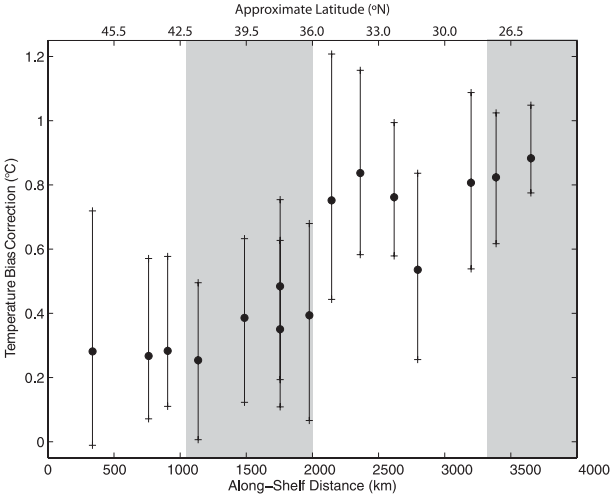

FIG. A1. Annual average bucket temperature bias correction estimates (circles) and seasonal range (crosses) along the U.S. East Coast. Bias correction estimates are made using the model of Folland and Parker (1995) and recent NDBC buoy observations of wind, SST, air temperature, and dewpoint. Along-shelf regions are shaded.

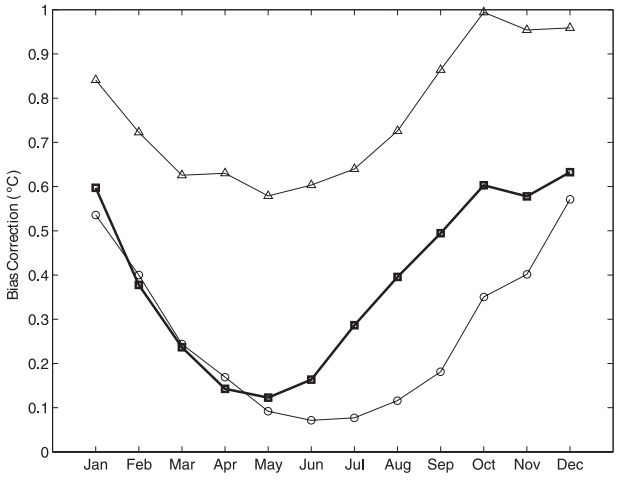

FIG. A2. Monthly regional bucket temperature bias corrections applied to the historical observations in this analysis for GOM (circles), MAB (squares), and SAB/FL (triangles).

APPENDIX

Bucket Temperature Bias Correction

SST measurements from buckets suffer from a well-documented bias toward cooler temperatures, associated with heat loss from the canvas or wooden buckets during thermometer readings (Folland 2005; Folland and Parker 1995; Smith and Reynolds 2002). Here, we use the Folland and Parker (1995) model and recent (1980–2007) hourly observations of wind speed, SST, air temperature and dewpoint from the NDBC data to compute the monthly climatologies (when at least 3 yr of observations are available) of bias corrections along the U.S. East Coast, assuming similar uninsulated bucket dimensions and a 5 min exposure. The annual mean bias correction increases from about 0.3°C in the GOM to 0.8°C in the SAB and FL (Fig. A1). In addition, the bias corrections have a distinct seasonal cycle, typically with maximum values in December and minimum values in May or June. The bias correction values and latitudinal dependence are similar to the estimates of Folland and Parker (1995). Our estimates of monthly climatological bias corrections are applied to all bucket temperature observations (i.e., pre-1970 observations) before merging with recent data. The bias corrections are applied regionally for sites grouped in the GOM, MAB, SAB, and FL (Fig. A2).

Effects of the bias correction

Adjusting the historical bucket temperature observations to correct for the cool bias is critical to estimating accurate long-term SST trends. Without the correction, long-term trends north of Cape Hatteras indicate stronger warming, ranging from 0.7° to 2.0°C (100 yr)$^{-1}$. On average, uncorrected, long-term SST trends in the GOM and MAB are larger by 0.4° and 0.3°C (100 yr)$^{-1}$, respectively, an increase of about 40% (Table A1). The effect is more pronounced in the winter, with long-term wintertime SST trends in the GOM and MAB larger on average by 0.6° and 0.4°C (100 yr)$^{-1}$, leading to a few unrealistic SST trends above 3.0°C (100 yr)$^{-1}$. South of Cape Hatteras, average long-term trends estimated from uncorrected data indicate warming of 0.6° and 0.3°C (100 yr)$^{-1}$ for the SAB and FL. The north–south dichotomy remains, however, and south of Cape Hatteras long-term trends without the bucket correction are mostly (6 of 11 sites) not significantly different from zero

TABLE A1. Regionally averaged SST trends [°C (100 yr)$^{-1}$] for the complete merged dataset, the merged dataset uncorrected for bucket temperature biases, and the pre-1970 bucket measurements–only dataset.

Region	Full corrected	Full uncorrected	Pre-1970 bucket only
GOM	1.0	1.4	1.3
MAB	0.8	1.1	0.8
GOM and MAB	0.9	1.2	1.0
SAB	−0.1	0.6	0.0
FL	−0.3	0.3	−0.2
SAB and FL	−0.2	0.5	−0.1

or warming but at a lower rate compared to the north, ranging from 0.4° to 1.1°C $(100\ \text{yr})^{-1}$.

Another test of the success of the bias correction comes from comparing the secular trends using the complete merged dataset and long-term trends using only bucket temperature observations, thus removing the bias that comes from comparing bucket and electronic thermistor temperature measurements. Long-term trends computed using only historical bucket temperature observations over the 95-yr period from 1875 to 1970 reflect the same characteristics as the full merged 132-yr corrected dataset. North of Cape Hatteras, pre-1970 trends are significantly warming with average trends for the GOM and MAB of 1.0° and 0.8°C $(100\ \text{yr})^{-1}$; south of Cape Hatteras, there are few significant trends, with averages that indicate slight cooling of −0.1° and −0.3°C $(100\ \text{yr})^{-1}$ for the SAB and FL.

REFERENCES

Boicourt, W. C., J. W. J. Wiseman, A. Valle-Levinson, and L. P. Atkinson, 1998: The continental shelf of the southeastern United States and Gulf of Mexico: In the shadow of the western boundary current. *The Sea: The Global Coastal Ocean,* A. R. Robinson and K. H. Brink, Eds., Regional Studies and Syntheses, Vol. 11, John Wiley & Sons, 135–182.

Bumpus, D. F., 1957: Surface water temperatures along Atlantic and Gulf coasts of the United States. U.S. Fish and Wildlife Service Special Scientific Rep. on Fisheries 214, 153 pp.

Chapman, D. C., and R. C. Beardsley, 1989: On the origin of shelf water in the Middle Atlantic Bight. *J. Phys. Oceanogr.,* **19,** 384–391.

Easterling, D. R., T. R. Karl, E. H. Mason, P. Y. Hughes, and D. P. Bowman, 1996: United States Historical Climatology Network (U.S. HCN) monthly temperature and precipitation data. Carbon Dioxide Information Analysis Center Rep. ORNL/CDIAC-87, NDP-019/R3, 280 pp.

Fairall, C. W., E. F. Bradley, D. P. Rogers, J. B. Edson, and G. S. Young, 1996: Bulk parameterization of air-sea fluxes for Tropical Ocean-Global Atmosphere Coupled-Ocean Atmosphere Response Experiment. *J. Geophys. Res.,* **101,** 3747–3764.

Flint, W., 1989: *Lightships and Lightship Stations of the U.S. Government*. U.S. Coast Guard Historian's Office, 23 pp.

——, 1993: *A History of U.S. Lightships*. U.S. Coast Guard Historian's Office, 24 pp.

Folland, C., 2005: Assessing bias corrections in historical sea surface temperature using a climate model. *Int. J. Climatol.,* **25,** 895–911.

——, and D. E. Parker, 1995: Correction of instrumental biases in historical sea surface temperature data. *Quart. J. Roy. Meteor. Soc.,* **121,** 319–367.

Fratantoni, P. S., and R. S. Pickart, 2007: The western North Atlantic shelfbreak current system in summer. *J. Phys. Oceanogr.,* **37,** 2509–2533.

Fung, I. Y., D. E. Harrison, and A. A. Lacis, 1984: On the variability of the net longwave radiation at the ocean surface. *Rev. Geophys.,* **22,** 177–193.

Lee, T. N., W. J. Ho, V. Kourafalou, and J. D. Wang, 1984: Circulation on the continental shelf of the southeastern United States. Part I: Subtidal response to wind and Gulf Stream forcing during winter. *J. Phys. Oceanogr.,* **14,** 1001–1012.

Lentz, S. J., 2008: Observations and a model of the mean circulation over the Middle Atlantic Bight continental shelf. *J. Phys. Oceanogr.,* **38,** 1203–1221.

——, 2010: The mean along-isobath heat and salt balances over the Middle Atlantic Bight continental shelf. *J. Geophys. Res.,* in press.

——, K. Shearman, S. Anderson, A. Plueddemann, and J. Edson, 2003: Evolution of stratification over the New England shelf during the Coastal Mixing and Optics study, August 1996–June 1997. *J. Geophys. Res.,* **108,** 3008, doi:10.1029/2001JC001121.

Levitus, S., J. I. Antonov, T. P. Boyer, and C. Stephens, 2000: Warming of the World Ocean. *Science,* **287,** 2225–2229, doi:10.1126/science.287.5461.2225.

Loder, J. W., B. Petrie, and G. G. Gawarkiewicz, 1998: The coastal ocean of northeastern North America: A large-scale view. *The Sea: The Global Coastal Ocean,* A. R. Robinson and K. H. Brink, Eds., Regional Studies and Syntheses, Vol. 11, John Wiley & Sons, 3–27.

Maul, G. A., A. M. Davis, and J. W. Simmons, 2001: Seawater temperature trends at Usa Tide Gauge sites. *Geophys. Res. Lett.,* **28,** 3935–3937.

Mountain, D. G., 2003: Variability in the properties of Shelf Water in the Middle Atlantic Bight, 1977–1999. *J. Geophys. Res.,* **108,** 3014, doi:10.1029/2001JC001044.

——, G. A. Strout, and R. C. Beardsley, 1996: Surface heat flux in the Gulf of Maine. *Deep-Sea Res. II,* **43,** 1533–1546.

NDBC, 2003: Handbook of automated data quality control checks and procedures of the National Data Buoy Center. NDBC Tech. Doc. 03-02, 54 pp.

Nixon, S. W., S. Granger, B. A. Buckley, M. Lamont, and B. Rowell, 2004: A one hundred and seventeen year coastal water temperature record from Woods Hole, Massachusetts. *Estuaries,* **27,** 397–404.

Pietrafesa, L. J., J. M. Morrison, M. P. McCann, J. Churchill, E. Bohm, and R. W. Houghton, 1994: Water mass linkages between the Middle and South Atlantic bights. *Deep-Sea Res. II,* **41,** 365–389, doi:10.1016/0967-0645(94)90028-0.

Smith, T. M., and R. W. Reynolds, 2002: Bias corrections for historical sea surface temperatures based on marine air temperatures. *J. Climate,* **15,** 73–87.

——, and ——, 2005: A global merged land–air–sea surface temperature reconstruction based on historical observations (1880–1997). *J. Climate,* **18,** 2021–2036.

——, ——, T. C. Peterson, and J. Lawrimore, 2008: Improvements to NOAA's historical merged land–ocean surface temperature analysis (1880–2006). *J. Climate,* **21,** 2283–2296.

Stearns, F., 1965: Sea-surface temperature anomaly study of records from Atlantic coast stations. *J. Geophys. Res.,* **70,** 283–296.

Steele, M., W. Ermold, and J. Zhang, 2008: Arctic Ocean surface warming trends over the past 100 years. *Geophys. Res. Lett.,* **35,** L02614, doi:10.1029/2007GL031651.

Stroeve, J., M. M. Holland, W. Meier, T. Scambos, and M. Serreze, 2007: Arctic sea ice decline: Faster than forecast. *Geophys. Res. Lett.,* **34,** L09501, doi:10.1029/2007GL029703.

Trenberth, K. E., and Coauthors, 2007: Observations: Surface and atmospheric climate change. *Climate Change 2007: The Physical Science Basis,* S. Solomon et al., Eds., Cambridge University Press, 235–336.

U.S. Coast and Geodetic Survey, 1955: Surface water temperatures at tide stations, Atlantic coast, North and South America. U.S. Department of Commerce Coast and Geodetic Survey Special Publication 278, 69 pp.

Valiela, I., 1995: *Marine Ecological Processes*. Springer, 686 pp.

Williams, C. N. J., M. J. Menne, R. S. Vose, and D. R. Easterling, 2007: United States Historical Climatology Network (HCN) serial temperature and precipitation data. U.S. HCN Rep. ORNL/CDIAC-118, NDP-019.

Worley, S. J., S. D. Woodruff, R. W. Reynolds, S. J. Lubker, and N. Lott, 2005: ICOADS release 2.1 data and products. *Int. J. Climatol.,* **25,** 823–842.